Modern Gas Kinetics

THEORY, EXPERIMENT AND APPLICATION

EDITED BY

M.J. PILLING MA, PhD
Lecturer in Physical Chemistry
University of Oxford

I.W.M. SMITH MA, PhD
Professor of Physical Chemistry
University of Birmingham

Chapter A3
Applications of Theory to Bimolecular Reactions

G. HANCOCK

Blackwell Scientific Publications
OXFORD LONDON EDINBURGH
BOSTON PALO ALTO MELBOURNE

Chapter A3
Applications of Theory to Bimolecular Reactions

G. HANCOCK

A3.1 Introduction: Reaction dynamics

The detailed study of a bimolecular reaction—the ways in which energy (translational, internal, chemical) in the reactants is converted into that of the products—is the province of the reaction dynamicist with his armoury of molecular beam and laser techniques. Experiments on state-to-state reaction dynamics are considered in Chapter B2. Here we concentrate on the interpretation of molecular beam experiments in terms of the forces (potential energy surfaces) governing the molecular interactions, and review some key experiments which point towards the type of information on these interactions which can be extracted from observations of energy distributions in the products.

A3.2 Molecular beam experiments on reactive scattering

Molecular beam experiments can be conceived in which both internal and translational energies of reactants and products are selected. Most experiments using beams are limited to selection of initial directions and velocities of reactants, and measurements of velocity-resolved angular distributions of products. In these cases the pertinent information on the dynamics of scattering can be judged by looking at a contour plot of the product velocities, measured relative to the centre-of-mass of the collision pair. Such velocities are not measured directly in the laboratory, and transformations from the LAB to CM frame must first be carried out by methods which are tedious but standard.[1]

Figure A3.1 shows the type of result obtained for the reaction between K atoms and Br_2 molecules, and illustrates the scattering pattern observed for one particular type of reaction, that characterised by forward scattering, where the product containing the new bond (KBr) is scattered in a forward direction with respect to the centre-of-mass velocity of the incoming atom (K). K and Br_2 approach each other head on (this is the picture that an observer would see if he were sitting on the centre-of-mass of the system, taken as the origin in Fig. A3.1; remember that the velocity of the centre-of-mass remains constant during the collision event and this can be subtracted from the laboratory behaviour before and after the collision in order to allow the dynamics to be clearly visualised). The KBr product velocity

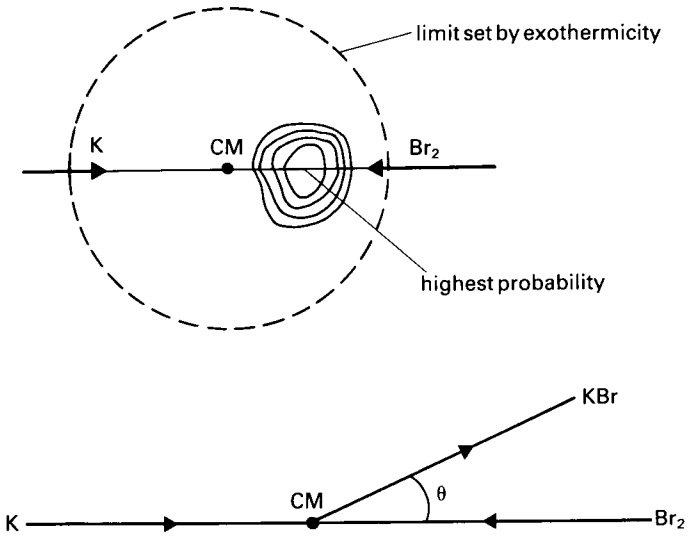

Fig. A3.1. Schematic contour diagram for the KBr product of the $K + Br_2$ reaction. Reactants approach each other head on in the centre-of-mass (CM) frame. With the position of the CM at the origin, the dashed circle shows the maximum value of the KBr CM velocity, determined from the reaction energetics. The solid contour lines show the observed KBr velocities, illustrating that forward scattering occurs (with respect to the K beam) and that the majority of the energy liberated in the reaction appears as internal excitation in the products.

is measured as a function of scattering angle from the initial straight line approach of the centre-of-mass velocities of K and Br_2, and is plotted as a contour diagram, with the height of the contour being proportional to the probability that a reactive event will end up with the KBr product velocity (a vector quantity having both magnitude and direction), with a value given by its coordinates. The dashed circle in Fig. A3.1 represents the maximum possible velocity of the KBr product, determined purely by energy conservation, i.e. the centre of mass velocity of KBr if *all* of the available energy appears as translation in the fragments.

The results for $K + Br_2$ show that the KBr product is scattered forward with respect to the initial direction of the K atom, and that the most probable translational energy is considerably smaller than the maximum possible—implying that most of the available energy appears as internal excitation in the products. These two features, plus the added observation that the reaction cross-section (proportional to the reaction probability) is large (50–200 $Å^2$), typify what is known as a stripping reaction, taking place by what has been called the harpoon mechanism. Figure A3.2 illustrates an explanation for two of these features, the magnitude of the reaction cross-section and the forward scattering dynamics. As neutral K

and Br_2 approach, the normal potential energy curve showing their interaction would be expected to show a small van der Waals minimum and then rise at short internuclear distance R. However, this curve will be crossed, at an internuclear separation R_c, by an ionic curve showing the Coulombic attraction between K^+ and Br_2^-. Initially, at large R, the ionic curve lies above that for the neutral species (the ionisation energy, I_K, of K is greater than the electric affinity, E_{Br_2}, of Br_2), but naturally this curve falls at smaller but still appreciable values of R due to the Coulombic attraction between the oppositely charged species. At the critical distance R_c, the difference $I_K - E_{Br_2}$ is just balanced by the Coulombic interaction $e^2/4\pi\varepsilon_0 R_c$ (in this simple treatment we neglect dispersion forces). This leads to an estimate for R_c (~ 6 Å in this case) in good accord with the experimental reaction cross-section, if the latter is assumed to be equal to πR_c^2. What is envisaged is that at R_c, the distance at which the electron transfers, Coulombic attraction leads automatically to reaction; the Br^-—Br bond is broken, and K^+ carries off a Br^- ion with no significant repulsion between the bromine atom and the bromide ion.

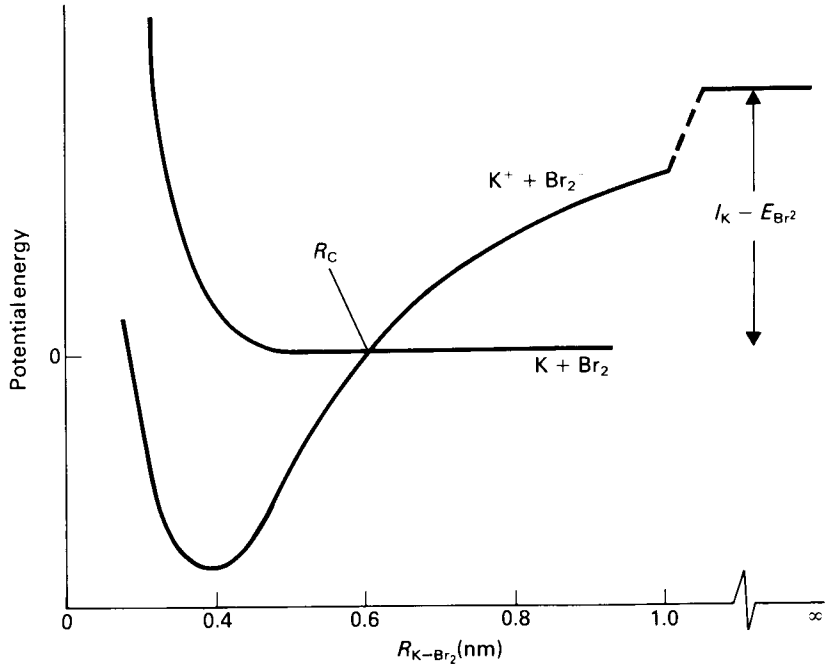

Fig. A3.2. Potential energy diagram to illustrate the harpoon model for the $K + Br_2$ reaction. Two schematic one-dimensional diabatic potential energy curves are shown, for the ionic ($K^+ + Br_2^-$), and covalent ($K + Br_2$) interactions, respectively. At large internuclear separation, the ionic curve lies above the covalent: the diabatic curves cross at R_c where the difference between the ionisation energy of K and the electron affinity of Br_2 is matched by the Coulombic attraction between the ions. Switching of potential curves at R_c leads to reaction with cross section $\sim \pi R_c^2$.

and Br_2 approach, the normal potential energy curve showing their interaction would be expected to show a small van der Waals minimum and then rise at short internuclear distance R. However, this curve will be crossed, at an internuclear separation R_c, by an ionic curve showing the Coulombic attraction between K^+ and Br_2^-. Initially, at large R, the ionic curve lies above that for the neutral species (the ionisation energy, I_K, of K is greater than the electric affinity, E_{Br_2}, of Br_2), but naturally this curve falls at smaller but still appreciable values of R due to the Coulombic attraction between the oppositely charged species. At the critical distance R_c, the difference $I_K - E_{Br_2}$ is just balanced by the Coulombic interaction $e^2/4\pi\varepsilon_0 R_c$ (in this simple treatment we neglect dispersion forces). This leads to an estimate for R_c (~ 6 Å in this case) in good accord with the experimental reaction cross-section, if the latter is assumed to be equal to πR_c^2. What is envisaged is that at R_c, the distance at which the electron transfers, Coulombic attraction leads automatically to reaction; the Br^-—Br bond is broken, and K^+ carries off a Br^- ion with no significant repulsion between the bromine atom and the bromide ion.

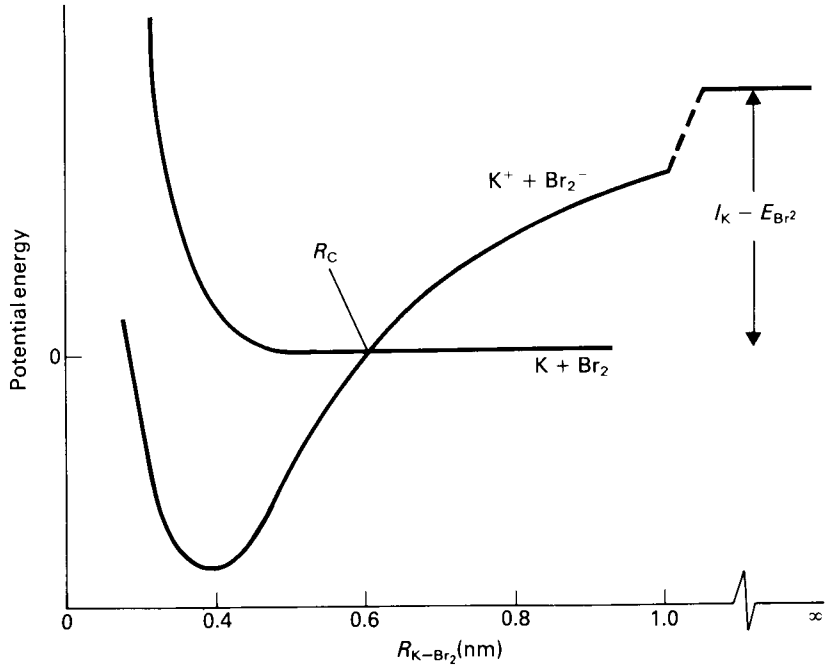

Fig. A3.2. Potential energy diagram to illustrate the harpoon model for the $K + Br_2$ reaction. Two schematic one-dimensional diabatic potential energy curves are shown, for the ionic ($K^+ + Br_2^-$), and covalent ($K + Br_2$) interactions, respectively. At large internuclear separation, the ionic curve lies above the covalent: the diabatic curves cross at R_c where the difference between the ionisation energy of K and the electron affinity of Br_2 is matched by the Coulombic attraction between the ions. Switching of potential curves at R_c leads to reaction with cross section $\sim \pi R_c^2$.

Thus the product is scattered in the direction of the incident K beam. This is the so-called harpoon model (the K atom throws the harpoon—the electron), with stripping (i.e. forward scattering) dynamics.

The observation that the majority of the available energy in the $K + Br_2$ reaction goes into internal excitation of the products might suggest an experiment designed to measure directly the distribution of this energy amongst the rotational and vibrational degrees of freedom of KBr. Laser induced fluorescence (see Chapter B1) would seem an obvious choice, but cannot be applied straightforwardly in this case, as KBr does not have a suitable bound upper state to be excited by the technique. Evidence for the extent of internal excitation has however been found by subsequent reactions of the KBr product. The process

$$KBr + Na \rightarrow K^* + NaBr$$

where K* is the first excited ^2P multiplet is $170\,kJ\,mol^{-1}$ endothermic, and thus could only occur with considerable excitation in the KBr reactant. The $190\,kJ\,mol^{-1}$ exothermicity of the $K + Br_2$ reaction can provide this excitation: emission from $K^*(^2P \rightarrow {}^2S)$ in a reacting mixture of K, Br_2 and Na has been observed and used to confirm the interpretation of the reactive scattering measurements.

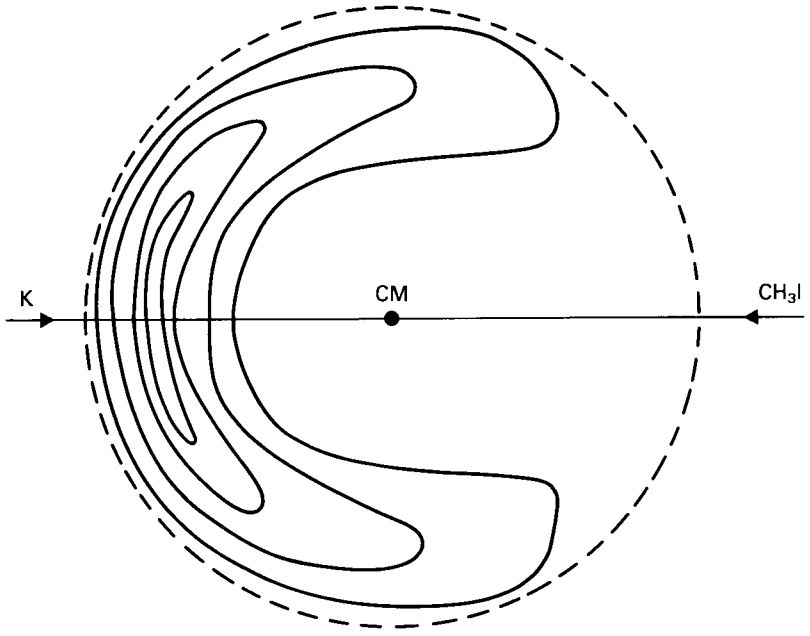

Fig. A3.3. Schematic contour diagram for the KI product of the $K + CH_3I$ reaction. Backward scattering with respect to the K beam occurs, with the majority of the available energy appearing as product translational energy.

A second type of scattering behaviour is typified by the process

$$K + CH_3I \rightarrow KI + CH_3.$$

Figure A3.3 shows a centre-of-mass contour diagram for the KI product. Here backward scattering is apparent, with a large fraction of the available energy appearing as product translation. Furthermore, the reaction cross-section is considerably smaller than in the $K + Br_2$ case (typically $< 50\,Å^2$ for a backward scattered process), and the dynamics imply that strong interactions only take place when reactants are closer to each other than in the $K + Br_2$ system.

A second example of 'rebound' dynamics, illustrating interesting behaviour, is shown in Fig. A3.4 for the reaction $F + D_2$. The DF product is back scattered, but in this case 'islands' of product intensity at specific values of the translational energy are seen, corresponding to the formation of vibrationally excited DF. There appears to be little rotational excitation in the product: if there was, then the vibrational states would not appear as resolved peaks in the translational energy distributions. The observations can be explained by considering the way in which product rotation arises in such a system. Conservation of angular momentum in the collision tells us that the angular momenta of the reactants and products must be equal. Two contributions towards the reactant angular momentum can be identified, namely that due to relative motion of the two species, l, and that due to rotational motion of the diatomic, j. In magnitude, $l = \mu u b$, where μ is the reduced mass, b the impact parameter and u the relative velocity. The first of these quantities is small for the $F + D_2$ system. The magnitude of j is also small for the widely spaced D_2 rotational levels populated at room temperature. The result is that there is little angular momentum in the reactant system, hence little to

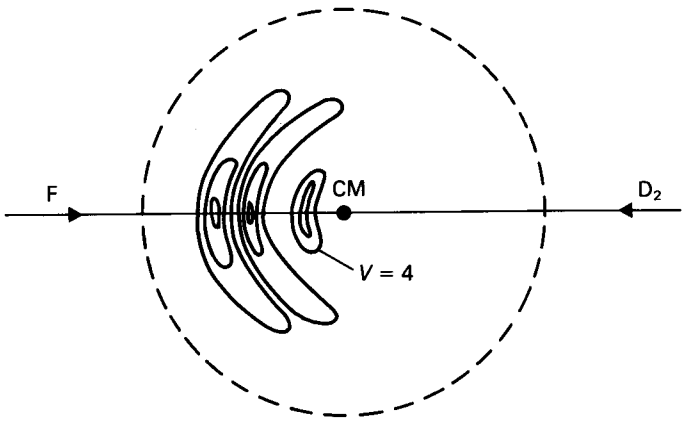

Fig. A3.4. Schematic contour diagram for the DF product of the $F + D_2$ reaction. DF is backscattered, and 'islands' of product intensity are seen corresponding to the formation of DF with up to four quanta of vibrational energy.

partition in the products and thus low rotational energy in the DF fragment. Reactions of this kind, in which internal state resolution is available via translational energy distributions, are rare but important, in that spectroscopic means of quantum state detection (by infrared chemiluminescence from the DF product in this case) can be used to check the results.

A third type of product scattering is observed in the reaction

$$Cs + SF_6 \rightarrow CsF + SF_5,$$

and Fig. A3.5 shows the contour diagram. Scattering here is seen to be symmetric in the forward and backward directions. What occurs is that a $CsSF_6$ collision complex is formed, and this lives for many rotational periods before breaking up into products, which show symmetric scattering about $\theta = 90°$. We shall see shortly that reactions of this kind can be treated theoretically in a relatively straightforward way to predict the distribution of energy in the products: a statistical distribution of some kind should appear if the complex lives long enough to allow equilibration of its internal degrees of freedom.

A3.3 State-to-state kinetics and potential energy hypersurfaces

Much information has now been gathered on the detailed dynamics of reactive scattering from the kind of results outlined above for molecular beam experiments, and from spectroscopic observations of product quantum states described elsewhere in Chapter B1. More details can be found in the general references[1–3] given at the end of this chapter. What controls the outcome of a chemical reaction is clearly the forces between individual atoms, represented by a potential energy

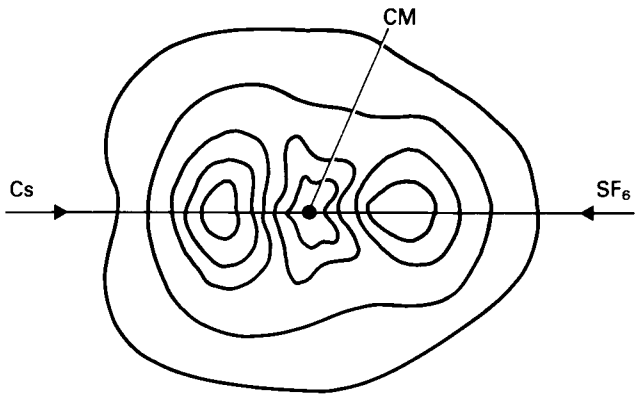

Fig. A3.5. Schematic contour diagram for the CsF product of the $Cs + SF_6$ reaction. Both forward and backward scattering of the CsF product are seen, corresponding to the formation of a long-lived complex.

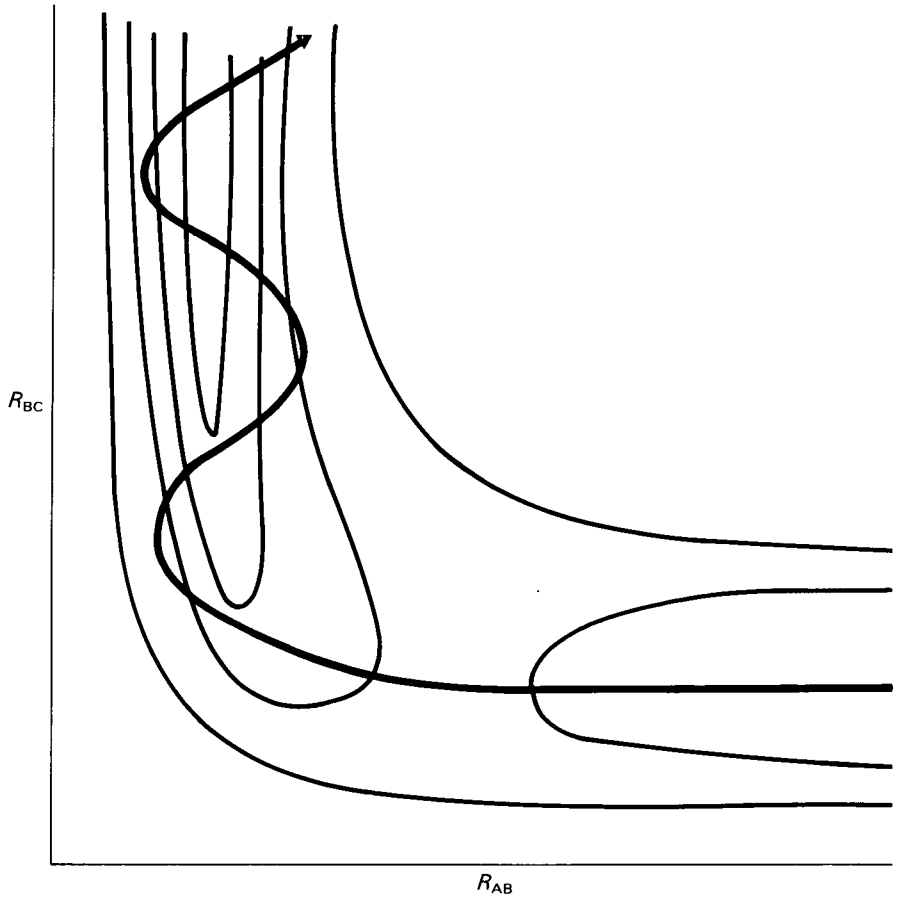

Fig. A3.6. Attractive potential energy surface for the reaction A + BC → AB + C. The activation energy barrier occurs in the entrance valley, with energy starting to be released at large R_{AB} and before R_{BC} has changed appreciably from its equilibrium value. Energy is channelled efficiently into vibrational excitation of the AB product, as shown by the trajectory in the exit valley.

surface (in an appropriate number of dimensions). Calculations of trajectories on a variety of different empirical surfaces have enabled some general conclusions to be drawn about the relationship between surface features and the scattering dynamics. Figure A3.6 illustrates one such case, for the reaction

$$A + BC \rightarrow AB + C$$

where reactants approach in a collinear fashion. The (small) activation energy barrier for this surface is seen to occur at a quite large value of R_{AB}, the distance between atoms A and B, and at a value of R_{BC} which is little different from its equilibrium value in the isolated molecule. This is a so called 'early barrier'; energy

starts to be released before R_{BC} changes appreciably, and trajectory calculations on the surface show that the outcome of the reaction is that energy is efficiently released as vibration of the AB product. This is termed 'attractive' energy release, and Fig. A3.6 shows what is generally described as an attractive potential energy surface. A second type of energy release, repulsive, occurs when the activation barrier is not in the 'entrance valley' as in Fig. A3.6, but in the 'exit valley', i.e. after the trajectory has turned the corner, and the B—C bond is being extended. Energy in this case is transferred more efficiently into translational motion of the products. Mixed energy release takes place by B—C repulsion whilst the nascent A—B bond is still extended from its equilibrium position. The extent of this release depends not only on the surface characteristics but also on kinematic effects due to the relative masses of the atoms.[2]

Intuitively it is satisfying to think of trajectories on a potential energy surface being represented by the motion of a point mass sliding over the topographical features in the way that a small sphere would move on a three-dimensional model of the surface. Figure A3.6 does not quite represent this motion correctly: in order to do this the axes need to be scaled and skewed, and the effect of skewing is shown in Fig. A3.7. The skew angle, χ, depends upon the relative masses of the atoms A, B and C and is given by equation 6 of Chapter A1:

$$\chi = \tan^{-1}[m_B(m_A + m_B + m_C)/m_A m_C]^{1/2}.$$

Figure A3.7 shows a trajectory on a surface with small χ appropriate for a mass combination of heavy (H) and light (L) atoms reacting according to

$$H + LH \rightarrow HL + H.$$

In Fig. A3.7 the surface that is illustrated is largely repulsive ('late barrier' in the exit valley), yet considerable vibrational excitation occurs in the AB product because of the kinematic effect of the point mass rounding the tight turn near the activation barrier. Such dynamical mass effects apparently operate in the reactions:

$$Cl + HI \rightarrow HCl + I,$$

and

$$H + Cl_2 \rightarrow HCl + Cl$$

for which the values of χ are 10.7° and 83°, respectively. Both surfaces are probably 'repulsive', yet in the first of these considerably more energy is converted into HCl vibration than in the second.

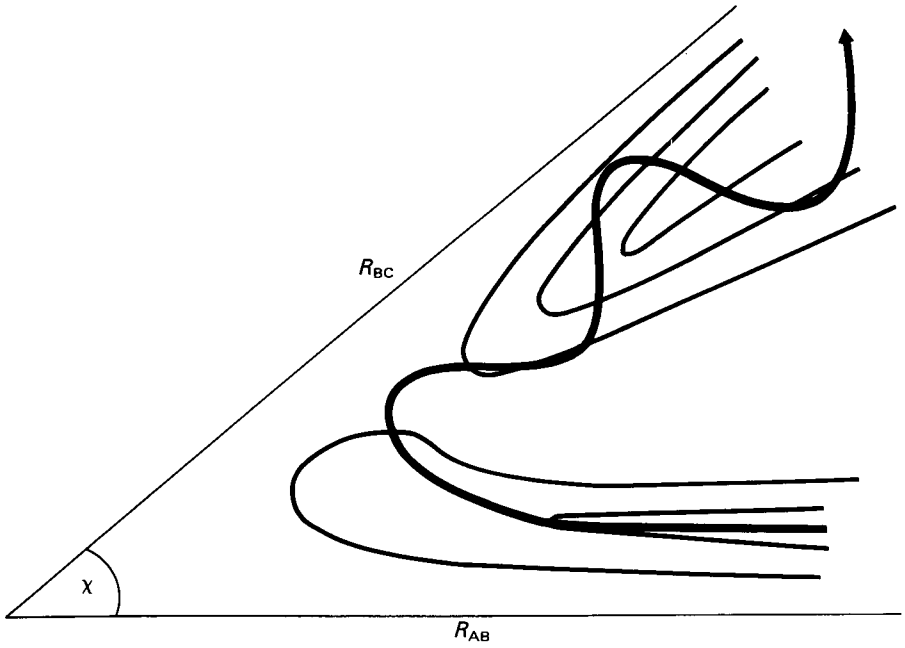

Fig. A3.7. The effect of skewed axes. A predominantly repulsive surface can channel energy efficiently into vibration in the products due to the nature of the trajectory turning the tight corner as energy is released.

Classical mechanics is, for most cases, satisfactory in determining trajectories on potential energy surfaces. Such trajectories can of course run backwards as well as forwards, and thus should be able to give information on the way in which reactant excitation can overcome potential energy barriers from observations of product excitation in the reverse reaction. For example, the reaction

$$Cl + HBr \rightarrow HCl(v') + Br \qquad \Delta H_0^{\ominus} = -69\,kJ\,mol^{-1}$$

produces vibrationally excited HCl in a population inversion with relative populations for $v = 0 : 1 : 2$ of $0.6 : 1.0 : 0.4$. Vibrational excitation in HCl(v) should thus be efficient in overcoming the activation barrier for the reverse (endothermic) process

$$Br + HCl \xrightarrow{k_v} HBr + Cl \qquad \Delta H_0^{\ominus} = 69\,kJ\,mol^{-1}.$$

Specific rate constants k_v for this process have been measured, in experiments in which HCl(v) was produced by prereaction of Cl atoms with HI[4] or by direct optical excitation.[5] What is of dynamical interest is how efficiently a specific form of energy is used to overcome a barrier—vibrational excitation of a reagent increases the total amount of energy available, but would an increase in rate

constant also have occurred if the same amount of energy was present in relative translation of the reactants? A case where the different efficiencies of these two forms of energy have been clearly demonstrated is for the reaction

$$K + HCl(v) \rightarrow KCl + H. \qquad \Delta H_0^{\ominus} \simeq 4\,\text{kJ mol}^{-1}.$$

Excitation of HCl to $v = 1$ increases the total cross-section for this reaction by about two orders of magnitude over that for the ground state reagents.[6] When the same amount of energy was put into the translational degrees of freedom of the reactants, the cross-section again increased, but by far less than that observed for vibrational excitation.

The effects of reagent rotation on reaction dynamics have been less studied than those for vibration or translation. For the $K + HCl$ $(v = 1, j)$ reaction, the cross-section is seen to decrease with increasing j.[7] Calculations on the $Li + HF$ reaction show an initial decrease of S_{reac} with increasing j, attributed to a preferred orientation of the reactions being disrupted as the rotational frequency increases, then followed by an increase in S_{reac}.[8] The latter effect was thought to be due to centrifugal distortion at high j increasing the HF bond distance and thus facilitating H atom abstraction.

Other examples of the effects of reagent excitation appear in Chapter B2, and have been comprehensively reviewed.[1,9] Space precludes their discussion here, except for a final example. This concerns the effect of reagent rotation on the product states of the reaction[10]

$$Ca + HF(v = 1, j) \rightarrow CaF(v'j') + H.$$

In this study it was found that increase in rotational quantum number, j, in HF simply seemed to have the effect of increasing the total energy in the system so that it could be distributed statistically in the internal states of the CaF product; as each $CaF(v')$ state became energetically accessible, it was formed. Energy distributions for reactions of this kind can be calculated with (almost) no knowledge of the potential energy surface controlling the reaction: what is required is that an intermediate 'complex' is formed which allows internal energy to be redistributed statistically amongst degrees of freedom of the products. Calculations can be performed at various levels of sophistication.

(a) Calculation of the prior distribution,[1] in which the probability of forming given product states is proportional to the statistical weight of the channel, i.e. for a rotational level j' the probability is proportional to $(2j' + 1)$, for a given translational energy E the probability is proportional to $E^{1/2}$.

(b) Phase space theory[11] (see section A4.8), in which the prior distribution is modified to allow for angular momentum conservation in the products—this needs to include some information on the long range attractive part of the (one-dimensional) intermolecular potential between the separating fragments.

(c) Statistical adiabatic channel theory[12] (see section A4.7), which is like phase

space theory except that the angular part of the intermolecular potential is also taken into account in deciding the way in which bending vibrations in the complex are converted to angular momentum.
Statistical theories such as these have been applied in some detail to the products of photodissociation and these applications have been recently reviewed.[13]

A3.4 Reagent alignment and orientation

Energy in reagents can overcome an activation energy barrier to reaction: intuitively it would seem reasonable to assume that the relative orientation of reagents, or the alignment of vector quantities associated with them (their rotational angular momentum for example) would also influence the dynamics. Partial orientation of the nuclear framework has been possible in molecular beam experiments, for example in the reaction

$$Rb + CH_3I \rightarrow RbI + CH_3.$$

Here the Rb prefers to attack the I end of the molecule[14]: attack within a cone of 45° angle at the C end of the molecule produces essentially no reaction. Care should be taken in formulating generalisations about such 'steric factors' however; no such asymmetry effect has been seen in the $K + CF_3I$ reaction[15] where immediate intuition would predict it. More recently orientation of reagents has been achieved by first forming a van der Waals complex between two molecules, then photolysing one of them to propel a fragment in a well-defined direction towards the other. The reaction

$$H + CO_2 \rightarrow OH + CO$$

has been studied in this way,[16] with photolysis of the HBr component of a weakly bound CO_2HBr complex providing the initial reagent orientation.

The absorption of radiation is an anisotropic process and can be used to produce species whose transition moments are aligned in the laboratory frame. For molecules, the transition moments are linked to the symmetry axes, and thus to the molecular framework, and absorption has been used to prepare species with some degree of alignment with respect to incoming reagents. An example is in the reaction

$$Sr + HF(v = 1) \rightarrow SrF + H$$

where absorption of polarised light from a laser was used to prepare $HF(v = 1)$ molecules so that their collisions with a beam of Sr atoms occurred either predominantly 'head on' or 'broadside'.[17] The latter configuration promoted reaction into

specific quantum states of SrF more efficiently.

Orbital (as opposed to nuclear framework) alignment has also been used to prepare reagents. An example is in the reaction

$$Ca(^1P_1) + HCl \rightarrow CaCl(B^2\Sigma^+, A^2\Pi) + H.$$

Polarised light was used to excite the $Ca(^1P_1 \leftarrow {}^1S_0)$ transition so that the p orbital lobes were aligned either along or perpendicular to the relative velocity vector of the reagents.[18] Some of the resultant emission from the excited CaCl states was found to depend upon this alignment, and a mechanism involving an electron jump model was able to reproduce qualitatively the observed effects.

Finally, we note that studies of alignment in the fragments of a 'half collision', i.e., photodissociation, are starting to provide an almost unprecedented amount of detail on the dynamics of an elementary process. As an example, we consider the photodissociation of HONO.[19] Quantum state-resolved observations of the OH product yields scalar information on the distribution of available energy into the degrees of freedom of the products, and vector information on the fragment recoil with respect to the transition moment, including orbital alignment, as revealed by the relative populations of the OH Λ doublets. Experiments of this kind on bimolecular collisions can be expected.

A3.5 Applications of theory to thermal rate data

In the remainder of this chapter, we consider how measurements of thermal rate data may be compared with the values of rate constants which are predicted theoretically. As Chapter A2 described, if the form of the potential energy surface is known, trajectories on the surface can be calculated; appropriate averaging for the range of collisions that are to be expected can be incorporated to produce a cross section, and thus a thermally averaged rate constant for comparison with measured data can be obtained. Naturally this approach also produces distributions of energy in the fragments (because the trajectories are classical, these have to be converted, as described in section A2.5, into suitable quantised distributions), and these can also be compared with the results of molecular dynamics experiments. For some simple reactions this has been done. For the simplest of all reactions

$$H + H_2 \rightarrow H_2 + H$$

an *ab initio* potential surface exists,[20] trajectory calculations have been run to produce cross-sections,[21] and during the last few years, quantum state-resolved product detection has been possible and experimental results for (v', j') distribu-

tions in the HD product of

$$H + D_2 \rightarrow HD + D$$

have been compared with those predicted theoretically.[22]

What happens if we do not have an *ab initio* potential energy surface to hand (which is certainly the case most of the time), and our main aim is understanding the magnitudes of thermal rate constants rather than quantum state distributions? We may apply transition state theory as outlined in Chapter A1. A bimolecular rate constant for the process

$$A + BC \overset{k}{\rightarrow} AB + C$$

is given by the expression

$$k = \left(\frac{k_B T}{h}\right) \frac{Q^{\neq}_{ABC}}{Q_A Q_{BC}} \exp\left(-\frac{\Delta E_0^{\neq}}{RT}\right) \tag{1}$$

where the Q's represent partition functions of the transition state and reactants, and $\Delta E_0^{\neq}$ is the appropriate zero-point energy difference between them. If we have a potential energy surface available, then k can be calculated—for example, $Q^{\neq}_{ABC}$ can be found by locating the transition state (as described in Chapter A.1), and thus obtaining its geometrical parameters, and by expanding the potential energy V around the transition state to obtain force constants, $k = -\partial^2 V/\partial y^2$, for motions orthogonal to the reaction coordinate and thus vibrational frequencies $\nu = (1/2\pi)(k/\mu)^{1/2}$. The correct surface will naturally reproduce the correct value of $\Delta E_0^{\neq}$ and thus the observed activation energy E_{act} for the process. Generally we need to proceed with approximate surfaces (or representations of the way the potential energy varies along the reaction coordinate) and use adjustable parameters in them to reproduce the experimentally observed activation energy, E_{act}. One such surface is the LEPS as described earlier (sections A1.2 and A2.2): we briefly mention below a second approach, the Bond-Energy-Bond-Order (BEBO) method which has been used for H atom transfer reactions involving linear transition states. Transition state calculations carried out using these approximate methods and an *ab initio* surface will then be compared with a series of experimental results.

The BEBO method[23] considers the electronic energy $V(R_1, R_2)$ along the path of minimum energy for the reaction

$$A + HB \rightarrow A \ldots\ldots H \ldots\ldots B \rightarrow AH + B$$

$$R_1 \qquad R_2$$

as being given by

$$V(R_1, R_2) = -E_1(\mathrm{AH}) - E_2(\mathrm{HB}) + E_3(\mathrm{AB})$$

where E_1 and E_2 are bonding interactions, and E_3 is an anti-bonding interaction: in E_1 and E_2 electron spins are anti-parallel, whereas they are parallel in E_3. For $E_1(\mathrm{AH})$, Pauling's empirical relationship between bond order n and bond length r is used:

$$E_1 = E_{1s}\, n^p$$

$$R_1 = R_{1s} - 0.26 \ln n$$

where E_{1s} is the bond energy for the isolated AH species of bond length R_{1s}, n is the bond order ($n = 0$ for no bond, $n = 1$ is for $R_1 = R_{1s}$, i.e. a complete AH diatomic bond) and p is an empirical constant.

It is assumed that the total bond order is one at all points along the reaction path, so that the HB bond energy is given by

$$E_2 = E_{2s}(1-n)^{p'}.$$

$E_3(\mathrm{AB})$ is an 'anti-Morse' function (see equation 3b in Chapter A2.2) representing the AB (triplet) repulsion energy. When empirical values of p and p' are assumed, then $V(R_1, R_2)$ can be evaluated for a number of values of n between 0 and 1 (i.e., as the reaction proceeds); the maximum value of $V(R_1, R_2)$ represents the activated complex. In practice, the thermal rate constants thus calculated will not generally have the right value of E_{act}, and the parameters p and p' are adjusted to rectify this.

Calculations of rate constants using the transition state theory approaches outlined above have been carried out for a number of systems, and in reference 24 a comparison has been made of experiment and theory for one of these, the reaction

$$\mathrm{OH} + \mathrm{H_2} \rightarrow \mathrm{H_2O} + \mathrm{H}.$$

In particular, the results of calculations on LEPS, BEBO and an *ab initio* surface were compared. Figure A3.8 shows the geometry of the HOHH transition state, with Table A3.1 indicating the differences between the molecular geometries found in the semi-empirical[25] and *ab initio*[26] approaches. In the former case, α, the H—O—H angle, was assumed to be as in the H_2O molecule, and β, the O—H—H angle, was assumed to be 180°: the *ab initio* results predict slightly different values for these angles, but bond lengths are in good agreement. What is of importance is the transition state predictions for the rate constants. In the semi-empirical case,

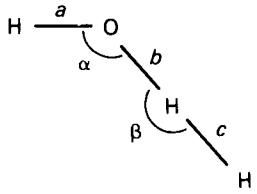

Fig. A3.8. HOHH transition state geometry for calculation on semi-empirical and *ab initio* surfaces. a, b and c are bond lengths, α the HOH bond angle, and β the OHH out-of-plane bond angle

calculations were made to fit the experimentally observed activation energies by varying the adjustable parameters (e.g., p and p' in the BEBO case). For the *ab initio* surface the correct activation energy should emerge, and this was found to be the case provided that $Q^{\neq}_{ABC}$ was evaluated accurately, not just in the rigid rotor harmonic oscillator approximation, and that a tunnelling correction was included.[26] Figure A3.9 shows the final results.[24] The experimentally determined rate constant for the reaction can be represented by the expression

$$k = 1.66 \times 10^{-16} (T/\mathrm{K})^{1.6} \exp(-1660\mathrm{K}/T)\ \mathrm{cm^3\ molecule^{-1}\ s^{-1}}$$

over the temperature range 300–2500 K, and both *ab initio* and semi-empirical calculations reproduce this functional form very well. However, caution is required in interpreting the results of the semi-empirical approach:[24] the frequencies and geometries may not truly represent the transition state (other structures may give the same rate constants) and the approximations made in the theory may give large inaccuracies. Methods of locating the transition state in both semi-empirical and *ab initio* surfaces, and of calculating its partition functions (including, for example, the effects of vibrational anharmonicities) have been reviewed.[27]

A3.6 Non-linear Arrhenius behaviour

As Fig. A3.9 shows, the Arrhenius plot for the $OH + H_2$ reaction is distinctly curved, i.e., the activation energy [as defined by $-\partial(\ln k)/\partial(1/\boldsymbol{R}T)$] is temperature dependent. We examine several possible causes of this.

Table A3.1. Calculated geometries for HOHH transition state

	BEBO[i]	LEPS[i]	*ab initio*[ii]
a/Å	0.96	0.96	0.98
b/Å	1.24	1.21	1.33
c/Å	0.85	0.85	0.85
α	104.6	104.6	97.6
β	180	180	165

(i) Reference 24, (ii) reference 26.

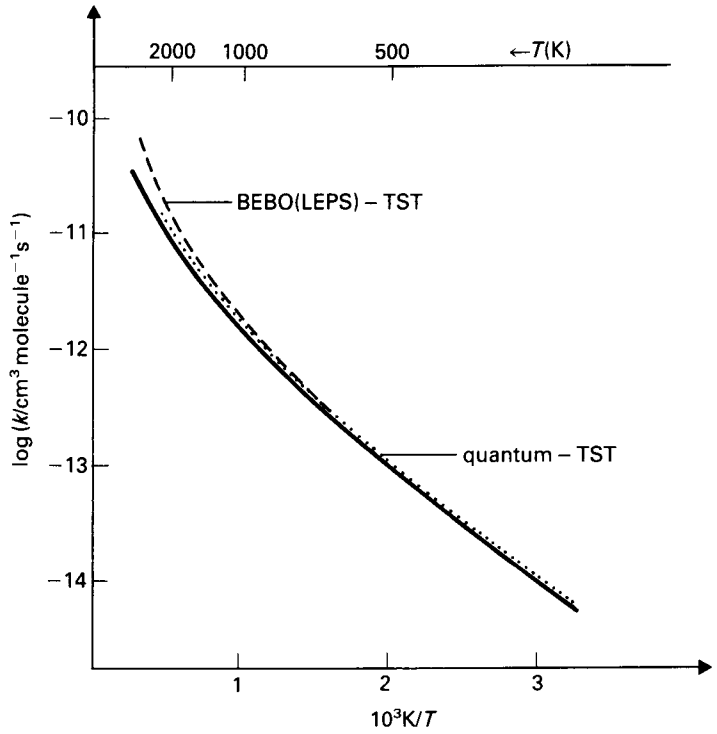

Fig. A3.9. Arrhenius plot for the $OH + H_2 \rightarrow H_2O + H$ reaction. The solid curve shows experimental results; the dashed curve (indistinguishable from the experimental results on this scale below ~600 K) is the semi-empirical transition states calculation using BEBO and LEPS surfaces; the dotted line is the *ab initio* calculation with a tunnelling correction. Adapted from reference 24 and reproduced with permission.

(i) State-specific rate constants

Enhancement of the cross-section of a chemical reaction by specific use of internal or translational energy in the reactants has already been mentioned. For the $OH + H_2$ reaction, rate constants have been measured for $H_2(v = 0)$ and $(v = 1)$, both yielding Arrhenius type expressions, but with different A factors and activation energies. As the temperature increases, and thus the contribution from reaction from $H_2(v = 1)$ increases, then the effective activation energy measured would be expected to change. One of the problems at the end of this chapter sets out the data, and the solution shows the curvature introduced. Vibrational excitation of $H_2(v = 1)$ increases the room temperature rate constant by a factor of approximately 120 over that for $H_2(v = 0)$,[28] whereas putting the vibrational energy into $OH(v = 1)$ only increases the room temperature rate constant by about 50%,[29] illustrating the intuitively satisfying idea that energy needs to be supplied to the

bond which will break in the chemical reaction. These effects can be understood at a more quantitative level employing the vibrationally adiabatic version of transition state theory that was outlined in section A1.4.

(ii) Temperature-dependent partition functions

The transition state theory formulation, equation 1, incorporates partition functions for reactants and activated complex, all of which will be temperature dependent in ways which are different for different degrees of freedom. For translational partition functions, Q_{tr} is proportional to $T^{3/2}$; for rotational partition functions Q_r is proportional to T for a linear species and to $T^{3/2}$ for a non-linear species, and the vibrational partition function for each harmonic oscillator is $Q_v = [1 - \exp - (h\nu/k_B T)]^{-1}$. The change in degrees of freedom in moving from reactants to activated complex will introduce temperature dependences into the ratio of the partition functions in equation 1 and leads to non-linearity in the Arrhenius plot: for the $OH + H_2$ reaction, the increase in activation energy between 300 and 2000 K due to the temperature dependence of partition functions has been estimated[24] to be 30 kJ mol^{-1}, a factor of two for this particular case.

(iii) Non-equilibrium behaviour

Our normal idea of a rate constant is that during the course of a reaction it remains invariant with time. However if, in the $OH + H_2$ reaction, the more rapidly reacting $H_2(v = 1)$ molecules were being depleted from the reactant mixture by chemical removal at a rate which was larger than the collisional re-establishment of Boltzmann equilibrium between $H_2(v = 0)$ and $(v = 1)$, then we would expect the measured rate constant to be time dependent, and not reflect the true (i.e., equilibrated reactants) thermal rate constant. Vibrational non-equilibrium effects of this kind have been calculated for the $OH + H_2$ reaction[24] and conditions identified where they introduce non-Arrhenius behaviour to the rate constants: they are only important when a substantial fraction of the reaction occurs via vibrationally excited states, and when vibrational relaxation is slow. Rotational and translational equilibria are in general more rapidly established than vibrational, and are assumed to be maintained in Boltzmann equilibrium in the reactants at all times.

(iv) Tunnelling

Non-linear Arrhenius behaviour due to quantum mechanical tunnelling (see section A1.5) will be most apparent for H atom transfer reactions at 'low' temperatures, where the bimolecular rate constant will be higher than that predicted classically. This effect is best seen in calculated rate constant values on *ab initio*

potential energy surfaces. For the $OH + H_2$ reaction, without a tunnelling correction, experiment[24] and theory[26] are in good agreement above ~ 1000 K, but diverge at lower temperatures, theory underestimating the measured rate constant by a factor of ~ 3 at 300 K. Inclusion of a tunnelling correction removes the discrepancy.[26] Reference 27 reviews the methods available using both semi-empirical and full quantum mechanical corrections.

A3.7 Entropies of activation and the prediction of *A*-factors

Equation 1 shows that, if the structure of the activated complex is known, then the bimolecular rate constant may be estimated via transition state theory. Reasonable guesses as to the structure may be made if no more theoretically sound method is available: this is normally done not through evaluation of partition functions but through estimation of entropies of activation. For a bimolecular process, such as

$$A + BC \rightarrow (ABC^{\neq}) \rightarrow \text{products}$$

the thermodynamic formulation of transition state theory expresses the rate constant as $k = (k_B T/h)K^{\neq}$, where $K^{\neq}$ is the equilibrium constant for formation of the activated complex. Since E_{act} is defined as $-\mathrm{d} \ln k/\mathrm{d}(1/\boldsymbol{R}T)$, it is related to the equilibrium constant, $K^{\neq}$, by the equation:

$$E_{act} = \boldsymbol{R}T - \mathrm{d} \ln K^{\neq}/\mathrm{d}(1/\boldsymbol{R}T).$$

Substituting for E_{act} in the normal Arrhenius expression enables the experimental A factor to be related to the entropy of activation, $\Delta S^{\neq}$, the difference in entropies between $ABC^{\neq}$ and reactants:

$$A = \mathrm{e}^2 \left(\frac{k_B T}{h}\right) \exp\left(\frac{\Delta S^{\neq}}{\boldsymbol{R}}\right)$$

where the standard state for $\Delta S^{\neq}$ is defined in concentration units (e.g. 1 molecule cm^{-3} or 1 mol cm^{-3}).[30]

The usual method of estimating $\Delta S^{\neq}$ is to start with an activated complex similar in structure to a stable molecule, whose third law entropy is known or can be calculated, and make appropriate corrections to allow for a 'looser' transition state than that found in the stable molecule, e.g., for changes in vibrational frequencies and symmetry. Benson's book 'Thermochemical Kinetics'[31] describes the approach in detail and we take an example from it, the bimolecular H-abstraction reaction

$$H + C_2H_6 \rightarrow C_2H_7^{\neq} \rightarrow H_2 + C_2H_5$$

to illustrate the entropic constraints placed on the A factor.

Contributions to $\Delta S^{\neq}$ may be assessed as follows, using C_2H_6 as a model for $C_2H_7^{\neq}$.

(a) The addition of a hydrogen atom makes a minimal difference to the mass and moments of inertia of C_2H_6, so that the contributions to the standard entropy of the complex, $S^{\ominus\neq}$, from translation and rotation, may be set equal to the contributions to $S^{\ominus}_{C_2H_6}$, with the addition of a term $\boldsymbol{R}\ln 6$, which takes into account the reduction in symmetry on forming the complex.
(b) A contribution of $\boldsymbol{R}\ln 2$ has to be added to account for the increase in electronic degeneracy on forming $C_2H_7^{\neq}$ (a doublet) from C_2H_6 (a singlet).
(c) Finally, there are changes in the vibrational and internal rotational partition functions consequent on forming H—H—C—. Benson[31] illustrates how these positive contributions to $S^{\ominus\neq}$ may be estimated, but we may set a lower limit on $S^{\ominus\neq}$ and on $\Delta S^{\neq}$ by neglecting them:

$$S^{\ominus\neq} \geqslant S^{\ominus}(C_2H_6) + \boldsymbol{R}\ln 12.$$

Thus

$$\Delta S^{\neq} \geqslant -S^{\ominus}(H) + \boldsymbol{R}\ln 12$$

which leads to an estimated A factor of $\geqslant 2 \times 10^{-11}$ cm^3 molecule^{-1} s^{-1}, an order of magnitude smaller than the experimental value of $\sim 2 \times 10^{-10}$ cm^3 molecule^{-1} s^{-1}. This discrepancy could be accounted for by the inclusion of the new bending vibrations and internal rotation in the partition function for the transition state and Benson obtains estimates of 2×10^{-10} cm^3 molecule^{-1} s^{-1} and 10^{-9} cm^3 molecule^{-1} s^{-1} for linear and non-linear H—H—C configurations in $C_2H_7^{\neq}$, respectively. It can be seen that calculations of this kind can be used to predict the pre-exponential factors for a variety of transition states, and hence to distinguish between various postulated microscopic mechanisms for the reaction.

A3.8 Conclusions

In recent years molecular beam and laser techniques have made the ultimate goal of chemical dynamicists just about possible—namely the measurement of cross-sections for fully state-selected reagents evolving into fully state-resolved products. Few reactions have had more than a part of their 'reaction space' probed, i.e., state resolution of products of thermal reactions has been extensively measured, as has velocity (but generally not internal states) of the products of angle-resolved molecular beam studies. These experiments can be expected to increase in sophistication and, will continue to test the theoriests' potential energy surfaces for the relatively simple systems for which both *ab initio* calculations and state-resolved experiments have been carried out. For systems with more than 'a few' atoms

(where 'few' is now perhaps 4 or 5) complications arise, both for theory and experiment (particularly when the effects of internal state distributions need to be evaluated). These reactions include many of importance in the applications of gas kinetics in, for example, combustion and aeronomy, and for these the main aim will still be the understanding and measurement of the thermally averaged rate constants.

A3.9 Suggestions for further reading

Bernstein R. B. (1982) *Chemical Dynamics Via Molecular Beam and Laser Techniques*, O.U.P.
Smith I. W. M. (1980) *Kinetics and Dynamics of Elementary Gas Reactions*, Butterworths, London.
Levy M. R. (1979) Dynamics of Reactive Collisions. *Prog. React. Kinet.*, **10**, 1.
Child M. S. (1986) Molecular Reaction Dynamics. *Sci. Prog. Oxf.*, **70**, 73.
Zellner R. (1984) Bimolecular Reaction Rate Coefficients. In *Combustion Chemistry*, (Ed. by W. C. Gardiner Jr.), p. 127. Springer Verlag, New York.
Benson S. W. (1976) *Thermochemical Kinetics*, Wiley, New York.

A3.10 References

1 Bernstein R. B. (1982) *Chemical Dynamics Via Molecular Beam and Laser Techniques*, OUP.
2 Levy M. R. (1979) Dynamics of Reactive Collisions. *Prog. React. Kinet.*, **10**, 1.
3 Child M. S. (1986) Molecular Reaction Dynamics. *Sci. Prog. Oxf.*, **70**, 73.
4 Douglas D. J., Polanyi J. C. and Sloan J. J. (1973) *J. Chem. Phys.*, **59**, 6679.
5 Arnoldi D. and Wolfrum J. (1976) *Ber. Bunsenges Phys. Chem.*, **80**, 892.
6 Odiorne T. J., Brooks P. R. and Kaspar J. V. (1971) *J. Chem. Phys.*, **55**, 1980.
7 Dispert H. H., Geis M. W. and Brooks P. R. (1979) *J. Chem. Phys.*, **70**, 5317.
8 Noorbatcha I. and Sathyamurthy N. (1982) *J. Am. Chem. Soc.*, **104**, 1766.
9 Kneba M. and Wolfrum J. (1980) *Ann. Rev. Phys. Chem.*, **31**, 47; Birely J. H. and Lyman J. L. (1975) *J. Photochem.*, **4**, 269.
10 Altkorn R., Bartoszek F. E., DeHaven J., Hancock G., Perry D. S. and Zare R. N. (1983) *Chem. Phys. Letters*, **98**, 212.
11 Pechukas P. and Light J. C. (1965) *J. Chem. Phys.*, **42**, 3281; Pechukas P., Rankin C. and Light J. C. (1966) *J. Chem. Phys.*, **44**, 794; Light J. C. (1967) *Disc. Faraday Soc.*, **44**, 14; Nikitin E. E. (1965) *Theor. Exp. Chem.*, **1**, 144; Klots C. E. (1971) *J. Phys. Chem.*, **75**, 1526; Klots C. E. (1972) *Z. Naturforsch., Teil A*, **27**, 553; Kinsey J. L. (1970) *J. Chem. Phys.*, **54**, 1206.
12 Quack M. and Troe J. (1974) *Ber. Bunsenges. Phys. Chem.*, **78**, 240; Quack M. and Troe J. (1975) *Ber. Bunsenges. Phys. Chem.*, **79**, 170; Quack M. and Troe J. (1981) *Int. Rev. Phys. Chem.*, **1**, 97.
13 Buelow S., Noble M., Radhakrishnan G., Reisler H., Wittig C. and Hancock G. (1986) *J. Phys. Chem.*, **90**, 1015.
14 Beuhler R. J. and Bernstein R. B. (1969) *J. Chem. Phys.*, **51**, 5305.
15 Brooks P. R. (1973) *Faraday Disc. Chem. Soc.*, **55**, 299.
16 Buelow S., Radhakrishnan G., Catanzarite J. and Wittig C. (1985) *J. Chem. Phys.*, **83**, 444.
17 Karny Z., Estler R. C. and Zare R. N. (1978) *J. Chem. Phys.*, **69**, 5199.
18 Rettner C. T. and Zare R. N. (1981) *J. Chem. Phys.*, **75**, 3636; (1982) **77**, 2416.

19 Vasudev R., Zare R. N. and Dixon R. N. (1984) *J. Chem. Phys.*, **80**, 4863.
20 Siegbahn P. and Liu B. (1978) *J. Chem. Phys.*, **68**, 2457.
21 Blais N. C. and Truhlar D. G. (1983) *Chem. Phys. Letters*, **102**, 120.
22 Marinero E. E., Rettner C. T. and Zare R. N. (1984) *J. Chem. Phys.*, **80**, 4142; Gerrity D. P. and Valentini J. J. (1985) *J. Chem. Phys.*, **82**, 1323.
23 Johnson H. S. and Parr C. (1963) *J. Am. Chem. Soc.*, **85**, 2544; Johnson H. S. (1966) *Gas Phase Reaction Rate Theory*, Ronald Press, New York.
24 Zellner R. (1984) Bimolecular Reaction Rate Coefficients. In *Combustion Chemistry*, (Ed. by W. C. Gardiner Jr.), p. 127. Springer Verlag, New York.
25 Smith I. W. M. and Zellner R. (1974) *J. Chem. Soc. Faraday Trans.* 2, **70**, 1045.
26 Schatz G. C. and Walch S. P. (1980) *J. Chem. Phys.*, **72**, 776.
27 See for example, Garrett B. C., Truhlar D. G. and Grev R. S. (1981) In *Potential Energy Surfaces and Dynamics Calculations*, (Ed. by D. G. Truhlar), p. 587 and references therein. Plenum Press, New York.
28 Zellner R. and Steinert W. (1981) *Chem. Phys. Letters*, **81**, 568; Glass G. P. and Chaturvedi B. K. (1981) *J. Chem. Phys.*, **75**, 2749.
29 Spencer J. E., Endo H. and Glass G. P. (1977) 16*th Symp. Combustion*, 829.
30 Golden D. M. (1971) *J. Chem. Ed.*, **48**, 235.
31 Benson S. W. (1976) *Thermochemical Kinetics*, Wiley, New York.

A3.11 Problems

Applications of theory to bimolecular reactions

A3.1. A 'prior' distribution for the internal energies of products of a chemical reaction can be calculated by writing down the *statistical* probability that particular quantum states can be formed. No dynamical effects are assumed: all energetically allowed product states are populated with a probability proportional to the number of states in the group.

For a reaction

$$A + BC \rightarrow AB(v', j') + C$$

write down the statistical probability of finding AB in a state (v', j') in terms of the available energy for partitioning into products (E), the vibrational energy $(E_{v'})$, and the rotational energy $[Bj'(j'+1)]$, (the degeneracy of translational states is proportional to the translational energy to the power 1/2).

Integrate this expression over j' (j' ranges from zero to some maximum value determined by energy conservation) to give an expression for the statistical probability $P^0(v')$ of finding AB in the *vibrational* level v', in terms of $E_{v'}$ and E. Assume that AB behaves as a rigid rotor. Now rewrite your expression in terms of $f = E_{v'}/E$, the fraction of available energy going into vibration. Normalise your expression by assuming AB is a harmonic oscillator, and that the energy levels are continuous, so that

$$\int_0^1 P^0(f)\, \mathrm{d}f = 1.$$

You should find

$$P^0(f) = \frac{5}{2}[1 - f(v')]^{3/2}.$$

Given the following data, calculate the experimental $P(v')$ values for the CO(v') product of O + CS and O + CSe reactions and plot them on the same graph as the prior distribution.

v'	$E(\mathrm{CO}, v')/\mathrm{cm}^{-1}$	Observed $P(v')$	
		O + CS	O + CSe
0	0	—	—
1	2143	—	—
2	4260	—	—
3	6350	—	—
4	8414	—	—
5	10452	—	—
6	12464	—	—
7	14449	0.1	—
8	16408	0.21	—
9	18342	0.49	—
10	20249	0.61	0.25
11	22131	0.73	0.40
12	23987	0.91	0.45
13	25817	1.00	0.47
14	27622	0.92	0.63
15	29401	0.30	0.74
16	31154	—	0.94
17	32882	—	0.94
18	34585	—	1.00
19	36263	—	0.66
20	37916	—	0.20

[Observed $P(v')$ are scaled to unity at maximum values]

For O + CS, $E = 376\,\mathrm{kJ\,mol^{-1}}$ ($31\,430\,\mathrm{cm^{-1}}$)

O + CSe, $E = 495\,\mathrm{kJ\,mol^{-1}}$ ($41\,377\,\mathrm{cm^{-1}}$).

A function often used to describe the distributions is a so-called 'surprisal plot'. The surprisal, $I[f(v')]$ is defined as

$$I[f(v')] = -\ln[P(v')/P^0(v')]$$

where $P(v')$ is the observed distribution and $P^0(v')$ the prior distribution. Calculate surprisals for each reaction and show that they vary linearly with $f(v')$.

A3.2. A calculation on the curvature introduced into Arrhenius type plots from vibrational enhancement of a simple reaction.
The reaction

$$OH + H_2(v) \rightarrow H_2O + H$$

has rate constants for $v = 0$ and 1 given by

$$k_0 = 9.3 \times 10^{-12} \exp(-18\,000/\boldsymbol{RT})$$

$$k_1 = 6.0 \times 10^{-11} \exp(-11\,000/\boldsymbol{RT})$$

where the rate constants are expressed in units of $cm^3\,molecule^{-1}\,s^{-1}$ and the activation energies are in $J\,mol^{-1}$. Calculate the rate constants expected for a Boltzmann vibrational distribution in the reactants at temperatures between 300 and 2500 K and plot the results in the usual Arrhenius form.

A3.12 Answers to problems

Applications of theory to bimolecular reactions

A3.1. The probability $P^0(v', j')$ of finding AB in a state (v', j') will be proportional to

$$(2j' + 1)[E - E_{v'} - Bj'(j' + 1)]^{1/2}.$$

The two terms represent (a) the degeneracy of the AB rotational level, and (b) the density of the translational states (the term in the square brackets being the energy available for partitioning into translation).

For a probability $P^0(v')$ we integrate this expression from $j' = 0$ to j'_{max}, where j'_{max} is given by $(E - E_{v'}) = Bj'_{max}(j'_{max} + 1)$. We assume rotational energy levels are continuous. The result is

$$P^0(v') = \frac{2k}{3B}(E - E_{v'})^{3/2}.$$

where k is a proportionality constant.

Assume AB is harmonic, with $E_{v'} = v'\varepsilon$ and $E = v'_{\max}\varepsilon$. Substituting $f = E_{v'}/E$, we find

$$P^0(f) = \frac{2k}{3B}(\varepsilon v'_{\max})^{3/2}(1-f)^{3/2}$$

Normalising,

$$P^0(f) = \frac{5}{2}[1-f(v')]^{3/2}$$

(see reference 1).

Figures A3.10 and 11 show (a) prior distributions plotted as a function of $f(v')$, together with measured $P(v')$ values for both reactions, where the measured $P(v')$ have been scaled so that they sum to the same value as the prior; and (b) the surprisal plots for the two reactions.

The aim here is to illustrate the similarity between the two vibrational distributions, both of which are inverted and produce stimulated emission from the CO product.

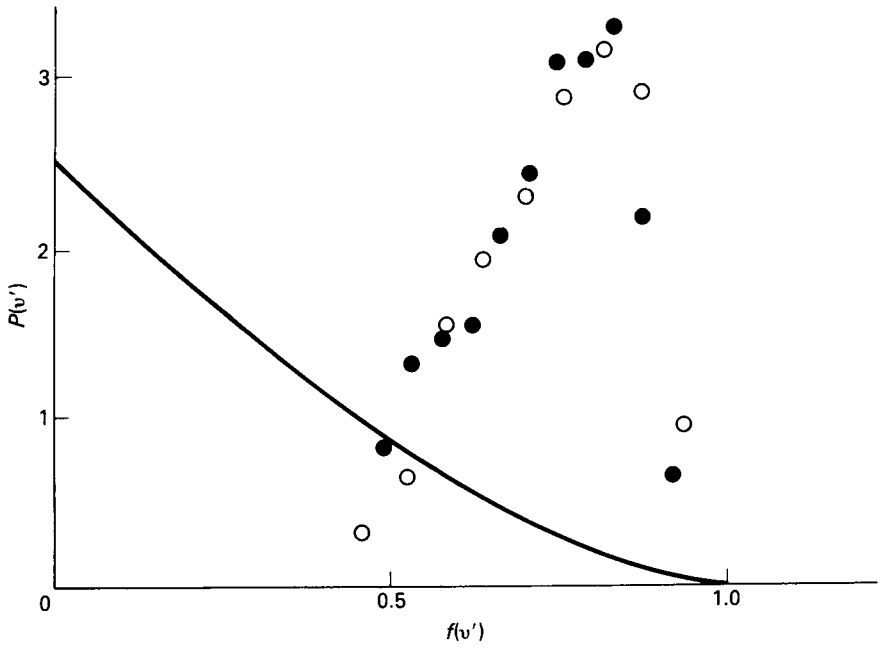

Fig. A3.10. Probability $P(v')$ of finding the product CO in the v'th vibrational level in the O + CS, CSe reactions: $f(v')$ is the fraction of the available energy appearing as vibration. The solid line is the prior distribution $P^0(v')$; the open and filled circles are the experimental values for the O + CS and O + CSe reactions, respectively.

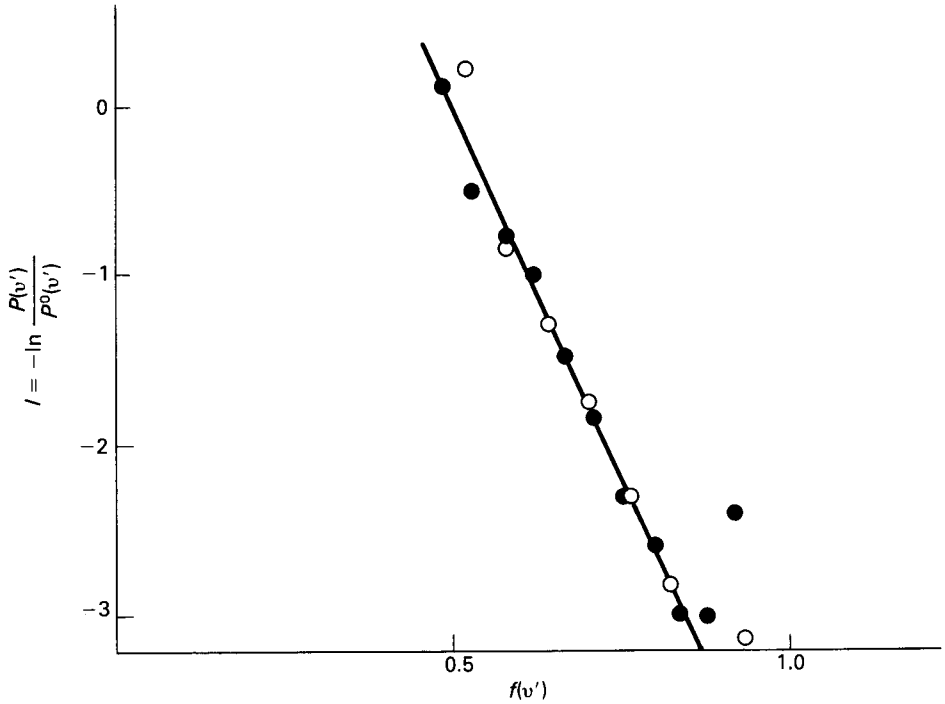

Fig. A3.11. Surprisal plot for the vibrational energy distributions in CO product of the O + CS (open circles) and O + CSe (filled circles) reactions. The surprisal I is defined as $I = -\ln P(v')/P^0(v')$, where $P(v')$ is the measured distribution and $P^0(v')$ the prior distribution. Points for both reactions lie on the same line, consistent with similar dynamics in the two cases.

For the original experimental data see Hancock G., Ridley B. A. and Smith I. W. M. (1972) *J. Chem. Soc., Faraday Trans.* 2, **68**, 2117; Morley C., Ridley B. A. and Smith I. W. M. (1972) *J. Chem. Soc., Faraday Trans.* 2, **68**, 2127.

A3.2. $k = \{k_0 + k_1 \exp[-\Delta E/\boldsymbol{R}T]\}/Q_v$

where $\Delta E = E[H_2(v=1)] - E[H_2(v=0)]$

$= 49.6\,\text{kJ mol}^{-1}$

$Q =$ vibrational partition function

$= [1 - \exp(-\Delta E/\boldsymbol{R}T)]^{-1}$.

(For discussion see Zellner R. (1984) Bimolecular Reaction Rate Coefficients. In *Combustion Chemistry*, (Ed. by W. C. Gardiner Jr.), p. 127. Springer Verlag.

The calculated temperature dependence of k is shown in Fig. A3.12 (overleaf).

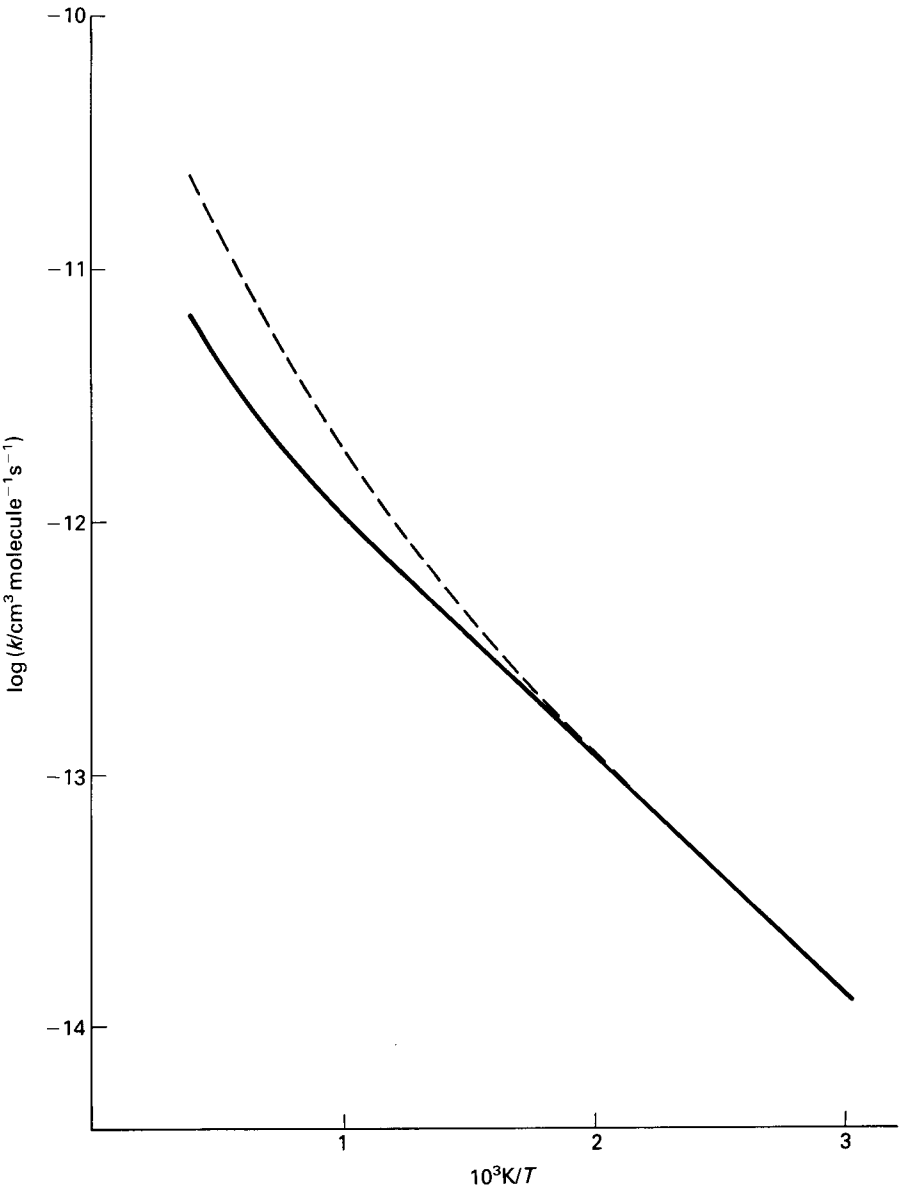

Fig. A3.12. Arrhenius plot of the thermal rate constant k for the $OH + H_2$ reaction. The solid curve is that calculated using measured state-specific rate constants for $H_2(v = 0)$ and $H_2(v = 1)$ as required in the problem. The dashed curve is the experimental variation of the thermal rate constant. Curvature is seen in both plots: the failure of the state specific rate constant at *high T* may be due to the assumption that at *low* temperatures the reaction proceeds without tunnelling: see reference 24 for details.